Adaptive Backstepping Control of Vacuum Servo System Using High-Speed on-off Valves

GANG YANG[1], **PENG JIANG**[1], **LEI LEI**[1], **YONG WU**[2], **JINGMIN DU**[1], **AND BAOREN LI**[1]

[1]School of Mechanical Science & Engineering, Huazhong University of Science and Technology, Wuhan 430074, China
[2]Wuhan Second Ship Design and Research Institute, Wuhan 430025, China

Corresponding author: Jingmin Du (hustdjm@hust.edu.cn)

ABSTRACT Using high-speed on-off valves (HSVs) with small size, low cost, and high switching accuracy instead of expensive proportional/servo valves, and researching high-performance vacuum servo system can further enhance the competitiveness of vacuum servo technology. However, due to the delay characteristics of high-speed on-off valve (HSV), the average gas mass flow rate of the output has dead zone, saturated zone and nonlinear zone. A linear compensation method for flow output is designed, so that the average gas mass flow rate of the output is approximately positively correlated with the duty cycle of the pulse width modulation (PWM) signal. Furthermore, because of the air compression and the leakage of the system, there exist parametric uncertainties, unmodeled dynamics and disturbances in the vacuum servo system. An adaptive backstepping control (ABC) strategy based on discontinuous projection mapping is designed. The adaptive backstepping control strategy inhibit the influence of system's parametric uncertainties through on-line update of the uncertain parameters, and uses its own robustness to eliminate the effects of unmodeled dynamics and disturbances. Compared with the sliding mode control (SMC) strategy, the experimental results show that when the tracking frequency reaches 3-4Hz, the adaptive backstepping control strategy can ensure good tracking performance.

INDEX TERMS Adaptive backstepping control, high-speed on-off valves, pulse width modulation, vacuum servo system.

I. INTRODUCTION

Pneumatic system has been widely used in robots, medical equipments and other industries because of its low maintenance cost, high power-weight ratio, cleanness and simple structure [1]–[4]. However, due to air compression, valve hysteresis, and nonlinear friction of actuators, the pneumatic system is a strong nonlinear system [5] and it is difficult to achieve high-precision control. With the occurrence and development of electrical proportional/servo valves, the pneumatic servo system has made a series of breakthroughs in tracking such as displacement [6], [7], speed [8], force [9], and pressure [10]–[14].

However, due to the disadvantages of high cost, large volume, and poor anti-pollution ability of the proportional/servo valves, the use of HSVs instead of proportional/servo valves has become a trend. The HSV has the advantages of fast

switching ability, low price, strong anti-pollution ability and high repeatability. Therefore, it is increasingly favored by researchers. In addition, the use of HSV instead of proportional/servo valve can effectively avoid the problems of temperature drift, zero drift and hysteresis caused by the existence of analog circuit in the control loop.

In order to obtain a continuous behavior from a pneumatic system using HSVs, the controller output signal is introduced to the system via a PWM scheme (converting control signals to "on/off" time intervals for each valve during a PWM period) in many pneumatic systems using HSVs [15].

Shen *et al.* [16] proposed a nonlinear model of pneumatic servo mechanism combined with PWM technology, which used the average mass flow to quantitatively describe the equivalent time dynamic response of PWM control. Sardellitti *et al.* [17] proposes a proportional ventilation scheme using HSVs for the small size, low cost and short switching time of the proportional ventilation system, useful for supplying high frequency ventilation through the driving

---

The associate editor coordinating the review of this manuscript and approving it for publication was Nishant Unnikrishnan.

circuit for the implementation of PWM control. As long as the input frequency of the PWM is high enough, HSVs can be approximated as a continuous input with proportional/servo valve control characteristics [18].

As the key technology of the hardware-in-the-loop simulation of high-altitude aircraft, vacuum pressure tracking control technology is mainly used to simulate the change of pneumatic pressure during flight of high-altitude aircraft [13]. The mass flow rate of the gas flowing into and out of the chamber is controlled by the pneumatic servo control technology, thereby controlling the pressure of the chamber. Jinyun *et al.* [19] proposed the pressure and vacuum continuous control system to change the pressure of the chamber in real time by controlling the electrical proportional/servo valve. Obviously, the higher the flying height of the aircraft, the higher the degree of vacuum.

Some researchers have proposed using nonlinear control algorithms in dealing with the nonlinearity of the vacuum servo system [20], [21]. Among them, Li *et al.* [20] introduced a feedback linearization-based self-tuning fuzzy PID controller to improve the performance of vacuum servo system, and the reference inputs are the square wave and sinusoidal with an amplitude of 0.4 kPa and frequency of 1 Hz. Cheng *et al.* [21] created a vacuum servo system using electro-pneumatic proportional directional valve that adopted adaptive robust controller to attenuate the effects of uncertain nonlinearities. Experimental results show that the proposed controller achieves the good tracking performance of dynamic pressure, when the pressure tracking range is from 20 kPa to 2 kPa and the sinusoidal pressure trajectories with amplitude of 0.4 kPa, frequencies of 2 Hz and 1 Hz. However, these studies used the expensive proportional/servo valve as the control element of the vacuum servo system.

Accordingly, Yang *et al.* [22] designed a dynamic vacuum pressure tracking system with HSVs that adopted SMC strategy to improve the performance and robustness of control for accurate dynamic vacuum tracking a sinusoidal signal with a frequency of 2Hz. However, the above research can only achieve tracking control with low frequency (≤2Hz) pneumatic pressure [20]–[22].

In order to widen the range of vacuum pressure tracking and improve the dynamic performance of the vacuum servo system. This paper proposes a higher frequency range of dynamic vacuum pressure tracking control, expanding the pneumatic pressure frequency from 1-2Hz to 1-4Hz, and use the HSVs as the control elements of the vacuum servo system.

As shown in Fig.1, the vacuum servo system consists of a vacuum pump, a chamber, two HSVs, two pressure sensors, a solid-state relay and a computer including the data acquisition card. During the experiment, the gas mass flow rate into and out of the chamber is changed by controlling the opening and closing state of the HSVs of the charging and discharging unit, and finally the change of chamber pressure is realized. The pneumatic pressure of vacuum pump and chamber are measured by pressure sensor 1 and sensor 2, respectively.
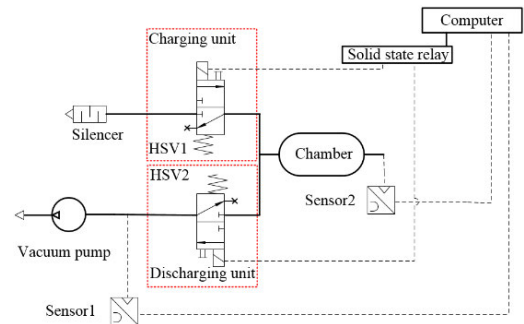

FIGURE 1. Schematic sketch of the vacuum servo system.

In order to improve the control accuracy of PWM-actuated HSVs, a number of approaches have been proposed to deal with the challenges of this system type such as SMC strategy [1], [18], [23], [24], and fuzzy control [25] using PWM-based control strategies. Jouppila Ville *et al.* [18] used the SMC strategy to provide a comparative study between PWM-actuated HSVs approaches and traditional servo valves approaches. Hodgson *et al.* [1], [23], [24] proposed a SMC strategy, systematically studied the dynamic control of cylinder displacement based on HSVs and designed 7 effective motion modes for 4-way HSV, which enables the precise position control of the cylinder under the lowest power condition of HSVs. Chandrapal *et al.* [25] proposed a novel implementation of a self-organizing fuzzy controller for the position and force control of a single pneumatic artificial muscle. Results show that the PWM-actuated HSVs performs better in response to abrupt changes.

However, previous researchs on HSVs focused on tracking control of displacement, speed and force. Rarely studied the tracking of HSVs in pneumatic pressure, especially vacuum pressure tracking control.

Due to the presence of uncertain nonlinearities of the vacuum servo system, the simplification of the thermodynamic process of the chamber and the change of the flow rate gain of the HSVs are called the parametric uncertainties of the system. The system's unmodeled dynamics and external disturbances cannot be established by mathematical models, which are called uncertain nonlinearities of the system. While the SMC strategy requires that the uncertainties of the nonlinear system are matched, and the unmatched uncertainties cannot guarantee the asymptotic stability of the system, which makes it difficult to satisfy many nonlinear uncertain systems [23]. At the same time, because of the discontinuity of sliding mode variable structure, the flutter phenomenon will appear in the practical application, which will cause the instability of the system.

The ABC strategy can eliminate the influence of the uncertain nonlinearities and solve the parametric uncertainties of the system. The robustness of the backstepping controller is used to inhibit the unmodeled dynamics and disturbances of the system to ensure the stable control effect of the system. so that the system has good steady-state control precision and

dynamic tracking performance. In the accurate tracking of pneumatic position, Yao *et al.* [26], [27] team made a series of research based on ABC strategy, and achieved fruitful results. In reference [26], to deal with the complexity and difficulties caused by the coupling and the appearance of parametric uncertainties in the input matrices, two backstepping designs via adaptive robust control Lyapunov functions are presented. In reference [27], the modularized adaptive backstepping designs are incorporated into the recently proposed adaptive robust control framework to synthesize indirect adaptive robust controllers that achieve not only good output tracking performance but also better parameter estimation processes to obtain accurate parameter estimates for secondary purposes. Deyuan *et al.* [28] built an adaptive robust controller based on discontinuous projection mapping. The nonlinear control algorithm designed by backstepping method was used to eliminate the influence of uncertainties in the control system. During the experiment, 0.5Hz sinusoidal signal was tracked, and the standard tracking error was less than 0.72mm.

The uncertainties of the vacuum servo system includes parameter uncertainties and uncertain nonlinearities. The virtual control input introduced by the backstepping controller is essentially a static compensation idea, which uses its own robustness to eliminate the influence of uncertainties and non-linearities of the system. However, the backstepping method can only ensure the transient performance of the system by giving a constant estimation value to the uncertain parameters when introducing the virtual control input. When there is only parameter uncertainties in the system, the adaptive controller guarantees the asymptotic stability of the system. However, this method does not consider the uncertain nonlinearities of the system and has poor robustness. Therefore, the adaptive backstepping controller combines the two controllers, not only ensuring the stable control effect of the system, but also taking into account the dynamic control performance of the system. Based on this, an ABC strategy is designed uses its own robustness to eliminate uncertain nonlinearities of the system in this paper, and then on-line update of the uncertain parameters in real time to eliminate the influence of the system's parametric uncertainties, thus ensuring the control performance of the system.

The organizational structure of this paper is as follows: The second part describes modeling and analysis, including system structure analysis, system model, mass flow linear compensation and multi-valves structure of discharging unit, the third part is the controller design, including duty cycle mapping scheme design and adaptive backstepping controller design. The fourth part is the experiments and analysis. Finally, conclusions are drawn in section "Conclusion".

II. MODELING AND ANALYSIS
A. SYSTEM STRUCTURE ANALYSIS
In order to analyze the relationship between the charging and discharging ability of the vacuum servo system shown in Fig.1. An analysis of the performance of system
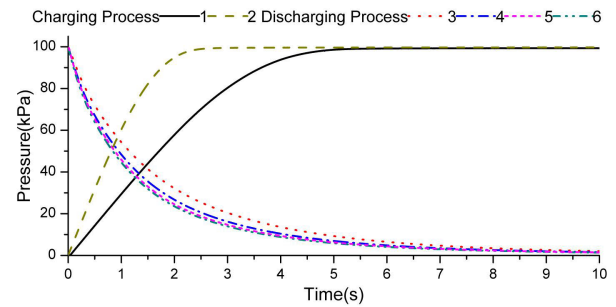
FIGURE 2. Experimental results of system charging and discharging performance for different charging and discharging units configurations.

charging and discharging was performed in actual experimental results. In Fig.2, two different specifications of HSVs with the same series were used, MHE2-MS1H-3/2G-1/8K (V1) and MHE3-MS1H-3/2G-1/8K (V2). The nominal sizes of V1 and V2 were 2 and 3 mm, respectively. During the charging process, one V1 and one V2 valve were used in producing curve 1 and curve 2, respectively. During the discharging process, only V2 valves were used, with curves 3–6 showing the results for the use of one to four valves, respectively.

As shown in Fig.2, it can be seen that the charging speed of curve 1 and curve 2 are greater than the discharging speed of curve 3. In balancing the charging ability of the charging unit and the discharging ability of the discharging unit, asymmetry is obviously suppressed in curve 1 and curve 5 in Fig.2, due to the respective choice of the smaller nominal HSV size in the charging unit and an increase in the number of HSVs in the discharging unit, which weakened system charging ability and strengthened system discharging ability. The multiple-valve structure of the discharging unit can thus satisfy the requirement of choosing the combination modes of the flow area, and thereby enable the flexible optimization of the balance between charging and discharging abilities by the controller. Due to the limitation of the pumping ability of the vacuum pump, the chamber pressure change rate in curve 6 is approximately equal to that recorded in curve 5 [22].

Based on the above experimental analysis, in order to balance the charging ability of the charging unit and the discharging ability of the discharging unit. As shown in Fig. 3, a schematic diagram of the asymmetric structure of the vacuum servo system is obtained(the discharging unit includes three V2 valves, and the charging unit has only one V1 valve). The system consists of one vacuum pump (Edwards Nxds15i), a chamber (FESTO-80-0.8-SAS0.73V-0.8L), 4 HSVs, 2 pressure sensors (Setra 270-RoHS), solid-state relays (Advantech PCLD-786) and a computer including the data acquisition card (Advantech PCI-1716).

During the experiment, the computer gets the pressure signal and then converts the calculated control law *u* into a PWM signal to drive the solid-state relays through PWM technology. Finally, *u* turns into a pulse signal [*U1, U2, U3, U4*] of HSVs.
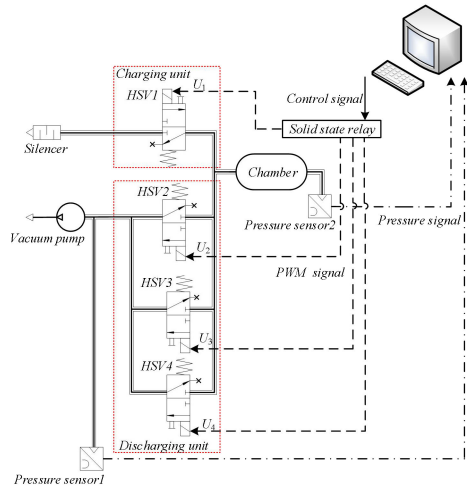
FIGURE 3. Schematic diagram of asymmetric structure of vacuum servo system.

B. SYSTEM MODEL

In a vacuum servo system based on proportional/servo valves control, the charging and discharging process of the system are independent [13]. During the actual system operation, there is only a separate charging or discharging mode. By controlling the gas mass flow of input and output of the chamber, precise control of the pressure in the chamber is realized. However, due to the discontinuous flow output of the HSVs, the same structure as the proportional/servo valves control vacuum servo system can not achieve better control effects. For the principle sketch of vacuum servo system shown in Fig.4, this paper designs a charging/discharging cooperative working mode, which realizes the pressure control of the chamber by controlling the difference between the gas mass flow of the input and output of the chamber.
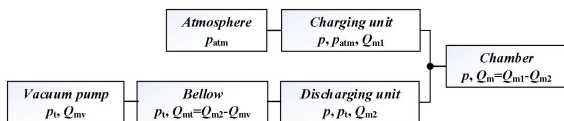

FIGURE 4. Principle sketch of vacuum servo system.

The mathematical model of the vacuum servo system includes gas source model, HSVs model, and the chamber model. It is assumed that the medium in the system is an ideal gas and satisfies the ideal gas state equation $p = \rho RT$, gas transmission process in the system is an isentropic adiabatic process, and the adiabatic coefficient $k = 1.4$. The mathematical model of the chamber can be expressed as:

$$\frac{dp}{dt} = \frac{kQ_m RT}{V} \tag{1}$$

where p is the pneumatic pressure of the chamber, R represents the gas constant given by $R = 287.1 \text{ Nmkg}^{-1}\text{K}^{-1}$, T is the temperature inside the chamber given by $T = 293$K, V represents the volume of the chamber and $V = 0.8$L. Q_m

represents the difference between the gas mass flow rate of the input and output of the chamber and $Q_m = Q_{m1} - Q_{m2}$, Q_{m1} and Q_{m2} indicate gas mass flow rate of charging and discharging unit respectively, they are described respectively as

$$\begin{cases} Q_{m1} = 0.0404 A_{cu} \dfrac{p_{atm}}{\sqrt{T}} f\,(p, p_{atm}) \\[2mm] Q_{m2} = 0.0404 A_{du} \dfrac{p}{\sqrt{T}} f\,(p, p_t) \end{cases} \tag{2}$$

where A_{cu}, A_{du} represent the effective cross-sectional areas of the HSVs of the charging and discharging units respectively. The positive pressure source is the ambient atmosphere given by $p_{atm} = 101.325$ kPa, p_t is the pressure in the intake of the vacuum pump.

$$\begin{cases} q_m = 0.0404 A \dfrac{p_1}{\sqrt{T}} f\,(p_1, p_2) \\[4mm] f\,(p_1, p_2) = \begin{cases} \sqrt{1 - \left(\dfrac{p_2/p_1 - \sigma}{1 - \sigma}\right)^2}, & p_2/p_1 > \sigma \\[4mm] 1, & p_2/p_1 \le \sigma \end{cases} \end{cases} \tag{3}$$

where q_m represents the gas mass flow rate of the HSVs, σ is the critical pressure ratio given by $\sigma = 0.26$. A is the effective cross-sectional areas of the HSV given by $A = \pi \alpha D x_v$ and D is the diameter of valve port, x_v is the spool displacement of the HSV, and α represents the correction coefficient of the flow area of the valve port given by $\alpha = 0.6$ [36], p_1, p_2 are the upstream and downstream pressure of the HSVs, respectively. During the charging process, $p_1 = p_{atm}, p_2 = p$ and during the discharging process, $p_1 = p, p_2 = p_t$.

The vacuum source contains the vacuum pump and the bellows. The mathematical model is as follows:

$$\begin{cases} Q_{mv} = \dfrac{p_t S_v}{RT}\left(1 - \dfrac{p_v}{p_t}\right) \\[3mm] \dfrac{dp_t}{dt} = \dfrac{kRT}{V_t}\,(Q_{m2} - Q_{mv}) \end{cases} \tag{4}$$

where p_t is the inlet pressure of the vacuum pump, S_v is the nominal pumping speed of the vacuum pump and $S_v = 15.1\text{m}^3/\text{h}$, p_v is the ultimate gas pressure of the vacuum pump and $p_v = 0.7$Pa, Q_{mv} is the pumping outflow of the vacuum pump and V_t is the volume inside the bellows given by $V_t = 1.3$L.

In the PWM-actuated HSVs controlled vacuum servo system, when the PWM signal output is 1, the flow area of the HSV is A ($A_e = 1*A$) and the flow output is q_m. When the PWM signal output is 0, the flow area of the HSV is 0 ($A_e = 0*A$) and the flow output is 0. The gas mass flow rate of the input and output of the chamber is in the form of a discrete gas flow package. Thus, when the package of mass flow rate is transmitted much faster than the system's own response characteristics within a period T_{pwm}, the system can approximate the average gas mass flow rate of the input and output in a continuous manner.

In a period T_{pwm}, the average gas mass flow rate $\bar{q}_m$ of the HSV is positively correlated with the average flow area $\bar{A}$, and the average flow area $\bar{A}$ is positively correlated with the spool duty cycle d. Therefore, the relationship between the average gas mass flow rate $\overline{q_m}$ and the spool duty cycle d is as follows:

$$\overline{q_m} = 0.0404\pi\alpha Dx_{vm}\frac{p_1}{\sqrt{T}}f(p_1, p_2)d \tag{5}$$

where x_{vm} represents the ultimate displacement of the HSV's spool. Thus, the average mass flow rates during the process of charging and discharging are described as

$$\begin{cases} \overline{Q_{m1}} = 0.0404A_{cu}\dfrac{p_{atm}}{\sqrt{T}}f(p_{atm}, p)d_{cu} \\ \overline{Q_{m2}} = 0.0404A_{du}\dfrac{p}{\sqrt{T}}f(p, p_t)d_{du} \end{cases} \tag{6}$$

where d_{cu} and d_{du} are the duty cycles for the process of charging and discharging, respectively.

Therefore, in a PWM cycle, the average mass flow rate in the chamber is described as:

$$\overline{Q_m} = \overline{Q_{m1}} - \overline{Q_{m2}} \tag{7}$$

From the above formula, we can get the mathematical model of the system as

$$\frac{dp}{dt} = \frac{k\overline{Q_m}RT}{V} \tag{8}$$

C. MASS FLOW LINEAR COMPENSATION

Although changes in HSV "on/off" operation would ideally take place instantly, the actual motion of the spool suffers from a delay. As shown in Fig.5, where T_{pwm} is the period of one PWM cycle, T_{on} is the high level of the input electrical signal in one PWM cycle, T_{son} is the time that the HSV receives the electrical signal U until the spool begins to move, T_{rise} is the time that the spool begins to move until the HSV opens completely, T_{soff} is the time that the HSV loses the electrical signal U until the spool begins to move back, and T_{fall} is the time that the spool begins to move back until the HSV closes fully.
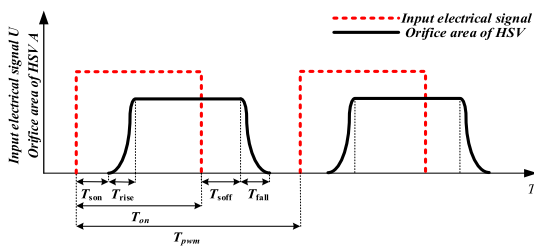

FIGURE 5. HSV on-off characteristics.

In order to eliminate the influence of the delay times T_{son}, T_{rise}, T_{soff} and T_{fall} on HSVs, it is assumed that T_{rise} is equal to T_{fall}, so that the corresponding gas mass flow rate is approximately equal and the gas mass flow rate at T_{rise} or T_{fall} is approximately half of that for a fully open HSV during the same time period. Since the average gas mass flow rate $\overline{q_m}$

of the HSV output is positively correlated with the average flow area $\bar{A}$. The method of flow output linear compensation is designed, which makes the average gas mass flow rate $\overline{q_m}$ of the HSVs output become approximately positively correlated with the PWM signal duty cycle w, and improves the control performance of the system.

In Fig.5, due to the delay characteristic of the spool, when the excitation voltage U is actually applied, the spool cannot be started immediately because there is a certain delay. Studying the effect of the HSV's delay on the average gas mass flow rate helps to improve the control performance of the vacuum servo system. Therefore, the simulation platform for relationship between duty cycle w of PWM signal and average gas mass flow $\overline{q_m}$ of HSV is built as shown in Fig.6.
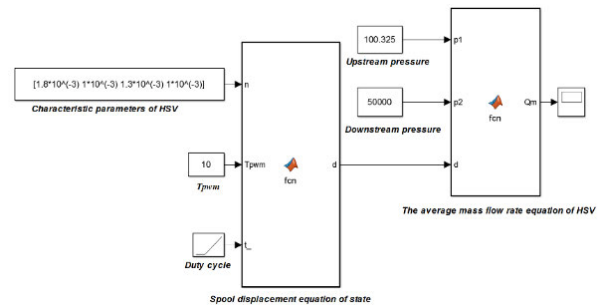

FIGURE 6. Simulation platform for relationship between duty cycle of PWM signal and average gas mass flow rate of HSV.

Through the simulation as shown in Fig.6, we can know the relationship between the duty cycle of PWM signal and average gas mass flow rate of HSV. HSVs' parameters of the FESTO MHE3 series are substituted into the above simulation platform, including the delay times $T_{\text{son}} = 1.8$ms, $T_{\text{rise}} = 1$ms, $T_{\text{soff}} = 1.3$ms and $T_{\text{fall}} = 1$ms, and the spool ultimate displacement $x_{\text{vm}} = 1.5$mm. During the simulation, the upstream pressure and downstream pressure of the HSV are 100.325 kPa and 50 kPa, respectively, the sampling period is 0.1ms, and the PWM signal period is $T_{\text{pwm}} = 10$ ms. The simulation results are as follows:

In Fig.7, it can be found that the average gas mass flow rate $\overline{q_m}$ of the HSV is not positively correlated with duty cycle w of PWM signal. There are dead zones, nonlinear zone 1, 2 and saturated zone that are not easily controllable. Moreover, the flow gain between the linear intervals is inconsistent. In order to eliminate the above-mentioned effects of nonlinear characteristics, method of mass flow linear compensation is designed as follows:

Step 1, the combination of the nonlinear zone 1 and the linear zone 1 is called a nonlinear zone A, and the linear zone 3 and the nonlinear zone 2 are combined as a nonlinear zone B.

Step 2, reduce the duty cycle range $[0, w_{\text{on}})$ of dead zone and nonlinear zone A to $[w_{\text{son}}, w_{\text{on}})$, and the conversion formula is:

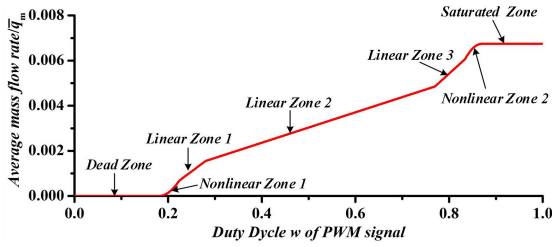$$w_c = \frac{w_{rise}}{w_{son} + w_{rise}}w + w_{son} \tag{9}$$

FIGURE 7. Characteristic chart of average gas mass flow rate of HSV.

Step 3, the duty cycle range $[1-w_{off},1]$ of the nonlinear B zone and saturated zone is reduced to $[1-w_{off},1-w_{soff}]$, and the conversion formula is:

$$w_c = \frac{w_{fall}}{w_{soff} + w_{fall}}w + \frac{w_{soff}}{w_{soff} + w_{fall}} - w_{soff} \qquad (10)$$

where $w_{rise} = T_{rise}/T_{pwm}$, $w_{son} = T_{son}/T_{pwm}$, $w_{fall} = T_{fall}/T_{pwm}$, $w_{soff} = T_{soff}/T_{pwm}$, $w_{on} = w_{son} + w_{rise}$, $w_{off} = w_{fall} + w_{soff}$.

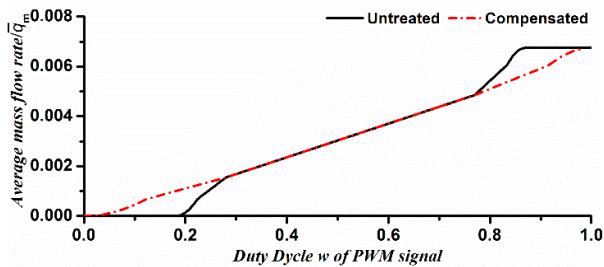Based on the the method of mass flow linear compensation, the simulation results are shown in the Fig.8.

FIGURE 8. Simulation results based on the method of mass flow linear compensation.

The simulation results show that the average gas mass flow rate $\overline{q_m}$ of the HSV is approximately positively correlated with duty cycle w of PWM signal after using the method of mass flow linear compensation. The influence of the flow gain inconsistency in the dead zone, the saturated zone and the linear zone is substantially eliminated. Obviously, the first segment and the end of the average gas mass flow rate $\overline{q_m}$ do not strictly satisfy the linear increasing relationship. From the previous HSV model analysis, it is because the spool duty cycle d and duty cycle w of PWM signal are in a quadratic functional relationship in the interval range. In essence, the method of mass flow linear compensation is a type of linear broadening method that does not eliminate the effects of second-order characteristics.

D. MULTI-VALVES STRUCTURE OF DISCHARGING UNIT

As shown in Fig.3, the charging unit adopts one V1 HSV and the discharging unit uses three V2 HSVs. Therefore, in order to establish relationship between the duty cycle d_{du} of discharging unit and the duty cycles d_{V2_1}, d_{V2_2} and d_{V2_3} of three V2 HSVs. It is assumed that the discharging unit is

a large valve, and the corresponding HSVs are sequentially activated according to the interval in which the duty cycle d_{du} is located. Therefore, the distribution algorithm of duty cycles of the discharging unit is designed as follows:

1. *if* $(d_{du} > 0)$ *and* $\left(d_{du} \leq {}^1/_3\right)$
   $d_{V2\_1} = 3d_{du}$, $d_{V2\_2} = d_{V2\_3} = 0$;
2. *if* $\left(d_{du} > {}^1/_3\right)$ *and* $\left(d_{du} \leq {}^2/_3\right)$
   $d_{V2\_1} = 1$, $d_{V2\_2} = 3\left(d_{du} - {}^1/_3\right)$, $d_{V2\_3} = 0$;
3. *if* $\left(d_{du} > {}^2/_3\right)$ *and* $(d_{du} < 1)$
   $d_{V2\_1} = 1$, $d_{V2\_2} = 1$, $d_{V2\_3} = 3\left(d_{du} - {}^2/_3\right)$;
4. *if* $(d_{du} == 0)$
   $d_{V2\_1} = d_{V2\_2} = d_{V2\_3} = 0$;
5. *if* $(d_{du} == 1)$
   $d_{V2\_1} = d_{V2\_2} = d_{V2\_3} = 1$; $\qquad (11)$

The open-loop control of the multi-valves structure of the discharging unit is shown in Fig.9. Through the distribution algorithm, duty cycle d_{du} of the discharging unit is converted into the duty cycles d_{V2_1}, d_{V2_2} and d_{V2_3} of HSVs. According to the conversion relationship between the duty cycle d of HSVs and the duty cycle w of the PWM signal, so that the PWM signal duty cycle w_{V2_1}, w_{V2_2} and w_{V2_3} of HSVs are obtained.
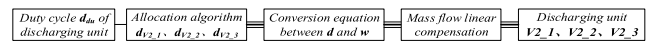

**FIGURE 9.** Open-loop control diagram of multi-valve structure of discharging unit.

The simulation results of multi-valves structure of discharging unit are as follows:

As shown in Fig.10(a), the HSVs of the discharging unit are sequentially activated in sequence. In Fig.10(b), the total average gas mass flow rate $\bar{Q}_{m2}$ of the discharging unit is approximately positively correlated with the discharging unit duty cycle d_{du}, but there is a flow fluctuation phenomenon at the circle mark in the figure. This is because the method of mass flow linear compensation cannot eliminate the quadratic functional relationship between the spool duty cycle d and the PWM signal duty cycle w.

III. CONTROLLER DESIGN
A. DUTY CYCLE MAPPING SCHEME DESIGN
Because of the charging and discharging units of the vacuum servo system are independent, the charging/discharging cooperative working mode is adopted. It is necessary to design a duty cycle mapping scheme to convert the control signal u into duty cycles d_{cu} of the charging unit and d_{du} of the discharging unit of the vacuum servo system respectively. Therefore, the duty cycle mapping scheme is designed as shown in Fig.11:
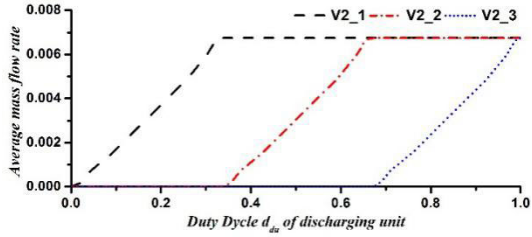
(a) Output average gas mass flow rate of the HSVs of the discharging unit
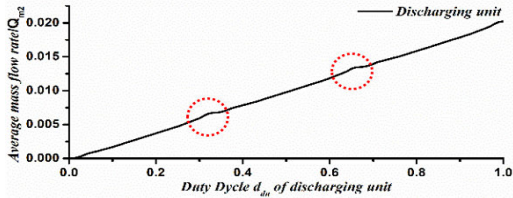
(b) Average gas mass flow rate of discharging unit

FIGURE 10. Simulation results of average gas mass flow in multi-valves structure of discharging unit.
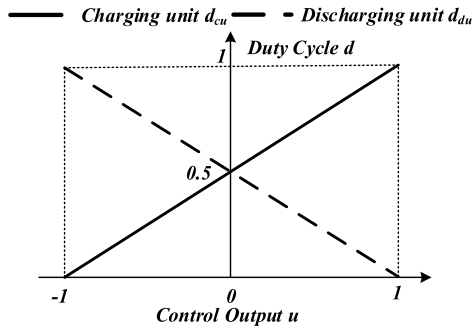

FIGURE 11. Duty cycle mapping scheme.

The specific instructions are as follows:

- When $u \in (-1, 1)$, $d_{cu} = 0.5u + 0.5$, $d_{du} = -0.5u + 0.5$.
- When $u = 1$, $d_{cu} = 1$, $d_{du} = 0$, the HSV of the charging unit is fully open, the HSVs of the discharging unit are all closed, and the charging capability is the strongest.
- When $u == -1$, $d_{cu} = 0$, $d_{du} = 1$, the HSVs of the discharging unit are fully open, the HSV of the charging unit is all closed, and the discharging capacity is the strongest.

B. ADAPTIVE BACKSTEPPING CONTROLLER DESIGN

Vacuum servo system is essentially a kind of nonlinear uncertain system. The system has parametric uncertainties, unmodeled dynamics and disturbances. Therefore, a mathematical model of the vacuum servo system considering unmodeled dynamics and disturbances is established, and then the adaptive controller is designed. Where the controller design includes two parts: the backstepping controller and discontinuous projection mapping. The robustness of the backstepping controller is used to inhibit the unmodeled dynamics and disturbances of the system to ensure the stable

control effect of the system. Then the uncertain parameters are identified by the on-line parameters updating of the adaptive law.

1) BACKSTEPPING CONTROLLER DESIGN

Establish a mathematical model of the vacuum servo system considering unmodeled dynamics and disturbances. Then, Eq. (8) can be rewritten in the following control form:

$$\frac{dp}{dt} = \frac{k\bar{Q}_m RT}{V} + d_n + \tilde{d}_0 \qquad (12)$$

where d_n is the nominal value of unmodeled dynamics and disturbances, $\tilde{d}_0$ is the high-frequency component of unmodeled dynamics and disturbances. Because of the nonlinear effect of the flow gain of HSV port, the relationship between the average gas mass flow rate of the actual chamber input and output is corrected as follows:

$$\bar{Q}_m = \lambda \left(\bar{Q}_{m1} - \bar{Q}_{m2} \right) \qquad (13)$$

where λ is the uncertain parameter of the average gas mass flow rate of the chamber, substitute Eq. (13) into (12), let $x = p$, in order to facilitate subsequent controller design, set the parameter vector $\theta = [\theta_1, \theta_2]^T$, where $\theta_1 = \lambda$ and $\theta_2 = d_n$, so that:

$$\dot{x} = \theta_1 \frac{kRT_S}{V} (\bar{Q}_{m1} - \bar{Q}_{m2}) + \theta_2 + \tilde{d}_0 \qquad (14)$$

Assumption 1: The parametric uncertainties, nominal value of the unmodeled dynamics and disturbances of the system are all bounded, satisfying the following relationship:

$$\begin{cases} \theta \in \Omega_\theta = \{\theta : \theta_{\min} \leq \theta \leq \theta_{\max}\} \\ |\lambda| \leq \lambda_{\max}, |d_n| \leq d_{n\_\max} \end{cases} \qquad (15)$$

where $\theta_{\max}$, $\theta_{\min}$ are the maximum and minimum parameter vector, $\lambda_{\max}$, $d_{n\_\max}$ are the maximum values of the parameters λ and d_n, respectively. Construct the Lyapunov energy function as follows:

$$V_1 = \frac{1}{2}e^2 \qquad (16)$$

where e is defined as the system tracking error given by $e = x - x_d$, and x_d represents the reference command signal. After the time derivation of V_1, Eq. (14) is substituted and obtained:

$$\dot{V}_1 = e \left[\theta_1 \frac{kRT_s}{V} \left(\bar{Q}_{m1} - \bar{Q}_{m2} \right) + \theta_2 + \tilde{d}_0 - \dot{x}_d \right] \qquad (17)$$

in Eq.(17), define $\bar{Q}_L = \bar{Q}_{m1} - \bar{Q}_{m2}$ as the virtual control input of the system, and construct the desired value $\bar{Q}_{Ld}$ of $\bar{Q}_L$:

$$\bar{Q}_{Ld} = \bar{Q}_{Lda1} + \bar{Q}_{Lda2} + \bar{Q}_{Lds1} + \bar{Q}_{Lds2} \qquad (18)$$

where $\bar{Q}_{Lda1}$ is the stable compensation item of the system, which uses the estimates set by uncertain parameters to improve and compensate the model. $\bar{Q}_{Lda2}$ is a fast dynamic compensation term, which is used to improve the system response speed and reduce the tracking error. $\bar{Q}_{Lds1}$ is a stable

feedback term of the system to ensure fast convergence of tracking error and robustness of the system. $\bar{Q}_{Lds2}$ is a fast robust feedback term for eliminating high-frequency component of unmodeled dynamics and disturbances. $\bar{Q}_{Lda1}$ and $\bar{Q}_{Lds1}$ are designed as follows:

$$\begin{cases} \bar{Q}_{Lda1} = \dfrac{V}{\hat{\theta}_1 kRT}\left(-\hat{\theta}_2 + \dot{x}_d\right) \\ \bar{Q}_{Lds1} = -\dfrac{V}{\hat{\theta}_1 kRT}\psi e \end{cases} \quad (19)$$

where $\widehat{\theta}_1$, $\widehat{\theta}_2$ are estimates of θ_1, θ_2 respectively, Ψ is the feedback gain of stable feedback term of the system and $\Psi > 0$,

substituting the expressions of $\bar{Q}_{Lda1}$ and $\bar{Q}_{Lds1}$ into Eq. (17) can be obtained:

$$\dot{V}_1 = -\psi e^2 + e[\dfrac{kRT}{V}\left(\hat{\theta}_1\bar{Q}_{Lda2} + \hat{\theta}_1\bar{Q}_{Lds2}\right) - \tilde{\theta}_1\alpha - \tilde{\theta}_2 + \tilde{d}_0] \quad (20)$$

where $\theta_i = \widehat{\theta}_i - \tilde{\theta}_i$, i = 1, 2, $\tilde{\theta}_i$ represents estimation error of the parameter θ_i, α is the estimation error coefficient of $\tilde{\theta}_1$ given by $\alpha = \frac{kRT\bar{Q}_L}{V}$. The $(-\tilde{\theta}_1\alpha - \tilde{\theta}_2 + \tilde{d}_0)$ term in the Eq. (20) concentrates the estimation error of the parameter vectors θ_1 and θ_2, it denotes the unmodeled dynamics and high-frequency component $\tilde{d}_0$ of the disturbances. Split $(-\tilde{\theta}_1\alpha - \tilde{\theta}_2 + \tilde{d}_0)$ into a nominal value ζ and a high-frequency component Δ as follows:

$$\zeta + \Delta = -\tilde{\theta}_1\alpha - \tilde{\theta}_2 + \tilde{d}_0 \quad (21)$$

Using the fast dynamic compensation term $\bar{Q}_{Lda2}$ to compensate the nominal value ζ and designed $\bar{Q}_{Lda2}$ expression is as follows:

$$\bar{Q}_{Lda2} = -\dfrac{V}{\hat{\theta}_1 kRT}\hat{\zeta} \quad (22)$$

where $\hat{\zeta}$ is the estimate of the fast dynamic compensation coefficient of the system. Substituting the Eq. (21) and Eq. (22) into the Eq. (20) can be obtained:

$$\dot{V}_1 = -\psi e^2 + e[\dfrac{kRT_s}{V}\widehat{\theta}_1\bar{Q}_{Lds2} + \Delta - \tilde{\zeta}] \quad (23)$$

where $\tilde{\zeta}$ is the estimation error of the fast dynamic compensation coefficient ζ. There exist a boundary in Eq. (23), and the boundary is set as:

$$h(x, t) = |\theta_{1M}||\alpha| + |\theta_{2M}| + d_{0M} \quad (24)$$

where θ_{1M} is the difference between the upper and lower bounds of the estimate of θ_1 is denoted as $\theta_{1M} = \widehat{\theta}_{1\_max} - \widehat{\theta}_{1\_min}$, θ_{2M} is the difference between the upper and lower bounds of the estimate of θ_2 is denoted as $\theta_{2M} = \widehat{\theta}_{2\_max} - \widehat{\theta}_{2\_min}$, and d_{0M} is the absolute value of the maximum value of the high-frequency component of the uncertain nonlinearities given by $d_{0M} = |\tilde{d}_{0\_max}|$. After using the continuous smooth sliding mode control strategy, the fast robust feedback

term $\bar{Q}_{Lds2}$ of the system to be determined can further weaken the influence of $(\Delta - \tilde{\zeta})$, designed as:

$$Q_{Lds2} = -\dfrac{V}{\widehat{\theta}_1 kRT}\dfrac{h^2(x, t)}{4\delta}e \quad (25)$$

where δ is the boundary layer thickness set by the fast robust feedback term $\bar{Q}_{Lds2}$ of the system to be determined. Substituting the Eq. (24) and Eq. (25) into the Eq. (23) can be obtained:

$$\begin{aligned} \dot{V}_1 &= -\psi e^2 + e[-\dfrac{h^2(x, t)}{4\delta}e + \Delta - \tilde{\zeta}] \\ &\leq -\psi e^2 + e[-\dfrac{h^2(x, t)}{4\delta}e + h(x, t)] \\ &= -\psi e^2 - \dfrac{1}{4\delta}(h(x, t)e - 2\delta)^2 + \delta \\ &\leq -\psi e^2 + \delta \end{aligned} \quad (26)$$

As can be seen from Eq. (26), if the control system must be progressively stable, then $\dot{V}_1$ must be greater than 0, and the converge to the sphere $e \leq \sqrt{\frac{\delta}{\psi}}$. Combining Eq. (17), Eq. (20), Eq. (21) and the expected value $\bar{Q}_{Ld}$ is:

$$\bar{Q}_{Ld} = \dfrac{V}{\widehat{\theta}_1 kRT}\left[\left(-\hat{\theta}_2 + \dot{x}_d\right) - \hat{\zeta} - (\psi + \dfrac{h^2(x, t)}{4\delta})e\right] \quad (27)$$

Combining Eq. (27) with the duty cycle mapping scheme as shown in Fig. 9 and the control law u can be obtained as:

$$u = \dfrac{2\frac{V}{\widehat{\theta}_1 kRT}\left[\left(-\hat{\theta}_2 + \dot{x}_d\right) - \hat{\zeta} - (\psi + \frac{h^2(x,t)}{4\delta})e\right] - (Q_{m1} - Q_{m2})}{Q_{m1} + Q_{m2}} \quad (28)$$

2) DISCONTINUOUS PROJECTION MAPPING

The $(\tilde{\theta}_1\alpha)$ term in the parametric estimation error varies with the system operation and is not a stable value. In order to compensate $(\tilde{\theta}_1\alpha)$ quickly, it is necessary to follow the system operation and change $\hat{\zeta}$ in Eq.(22) to improve the response speed of the system and ensure the tracking performance of the system. Based on the tracking error e, an adaptive function is designed, where the discontinuous projection is:

$$\dot{\hat{\zeta}} = Proj_{\hat{\zeta}}(\upsilon e) = \begin{cases} 0 & if\ \hat{\zeta} = \zeta_{max}\ and\ \upsilon e > 0 \\ 0 & if\ \hat{\zeta} = \zeta_{min}\ and\ \upsilon e < 0 \\ \upsilon e & otherwise \end{cases} \quad (29)$$

where υ is the adaptive law of the fast dynamic compensation coefficient ζ. ζ_{max}, ζ_{min} is the maximum and minimum estimate of ζ respectively. In Eq.(29), the discontinuous standard projection function is used to design the boundary constraint on the estimate of the fast dynamic compensation coefficient ζ, so that the parameter $\widehat{\zeta}$ after iteration is made within a preset range, and the parameter estimates is guaranteed to be in a stable range.

Furthermore, in Eq.(28), the uncertain parameters θ_1 and θ_2 use a constant estimate, and when the estimate is reasonable, a good control effect can be obtained. But when the

uncertain parameters change during the operation, constant estimates will make it difficult to ensure consistent control performance. Therefore, in order to inhibit the influence of parametric uncertainties, the adaptive law is used to update the estimates online. Based on the error feedback design method, the adaptive law of the uncertain parameter estimates is:

$$\dot{\hat{\theta}}_i = Sat(\dot{\hat{\theta}}_{iM}, \Pr oj_{\hat{\theta}}(\Gamma\gamma)), \quad i = 1, 2 \tag{30}$$

where $\Gamma = \mathrm{diag}(\rho_1, \rho_2)$ is matrix of the adaptive law, and the parameters ρ_1 and ρ_2 in the positive definite diagonal matrix determine the updating rate of the uncertain parameters θ_1 and θ_2. γ is matrix of the adaptive function given by $\gamma = [\gamma_1\gamma_2]^{\mathrm{T}}$. $\dot{\hat{\theta}}_{iM}$ is the maximum value of the update speed of the uncertain parameters θ_1 and θ_2. $Sat(\bullet)$ function limits the update speed of the uncertain parameters θ_1 and θ_2 using a saturation function. To ensure the stability of the adaptive control rate, the uncertainties of the system should be bounded, namely Assumption 1. The discontinuous projection is defined as:

$$\Pr oj_{\hat{\theta}}(\Gamma\gamma)$$
$$= \begin{cases} 0, & \hat{\theta}_i = \theta_{i\,\mathrm{max}} \text{ and } \Gamma\gamma > 0 \\ 0, & \hat{\theta}_i = \theta_{i\,\mathrm{min}} \text{ and } \Gamma\gamma < 0 \\ \Gamma\gamma, & \text{otherwise} \end{cases} \tag{31}$$

$$Sat\left(\dot{\hat{\theta}}_{iM}, \Pr oj_{\hat{\theta}}(\Gamma\gamma)\right)$$
$$= s\Pr oj_{\hat{\theta}}(\Gamma\gamma), \quad s = \begin{cases} 1, & \|\Gamma\gamma\| \le \dot{\hat{\theta}}_{iM} \\ \dfrac{\dot{\hat{\theta}}_{iM}}{\|\Gamma\gamma\|}, & \|\Gamma\gamma\| > \dot{\hat{\theta}}_{iM} \end{cases} \tag{32}$$

During the on-line update process, the estimates exceed the actual boundary, which will cause instability of the system. Therefore, limiting the boundary of estimates with discontinuous projection mapping. At the same time, in order to prevent the instability of the system caused by the excessive update rate of the estimates, the saturation function is used to limit the update speed of the parameter estimates. Based on the Lyapunov energy function, construct the following function below:

$$V_2 = V_1 + \frac{1}{2}\frac{\tilde{\theta}_1^2}{\rho_1} + \frac{1}{2}\frac{\tilde{\theta}_2^2}{\rho_2} \tag{33}$$

After differentiating Eq. (33), then:

$$\dot{V}_2 = -\psi e^2 + e\left[-\frac{h^2(x,t)}{4\delta}e + \Delta - \tilde{\zeta}\right]$$
$$+ \tilde{\theta}_1\left(\frac{1}{\rho_1}\dot{\hat{\theta}}_1 - \alpha e\right) + \tilde{\theta}_2\left(\frac{1}{\rho_2}\dot{\hat{\theta}}_2 - e\right) \tag{34}$$

In order to make $\dot{V}_2$ less than 0, the expressions of $\dot{\hat{\theta}}_1$ and $\dot{\hat{\theta}}_2$ are designed as follows:

$$\begin{cases} \dot{\hat{\theta}}_1 = \rho_1\alpha e \\ \dot{\hat{\theta}}_2 = \rho_2 e \end{cases} \tag{35}$$
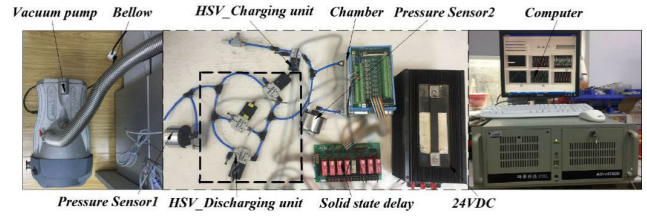

FIGURE 12. The photograph of the experimental setup.

Bringing the Eq. (35) into the Eq. (34), you can get:

$$\dot{V}_2 = -\psi e^2 - \frac{1}{4\delta}(h(x,t)e - 2\delta)^2 + \delta \le -\psi e^2 + \delta \tag{36}$$

From Eq. (36), the system is stable and the tracking error will converge to the sphere $e \le \sqrt{\frac{\delta}{\psi}}$.

3) ANALYSIS OF DESIGN PARAMETERS
The Eq. (36) is transformed:

$$V_2(t) \le e^{-2\psi t}V_2(0) + \frac{\delta}{2\psi}\left(1 - e^{-2\psi t}\right) \tag{37}$$

It can be seen from equations (36) and (37) that the larger the feedback gain ψ, the smaller the boundary layer thickness δ, the smaller the steady-state error of the system, and the shorter the response time of the transition process. Then it can be known from Eq.(14) and Eq.(18):

$$\dot{e} = -\left(\psi + \frac{h^2(x,t)}{4\delta}\right)e + \left(-\tilde{\theta}_2 - \tilde{\theta}_1\frac{kRT}{V}\bar{Q}_{Ld} + \tilde{d}_0 - \hat{\zeta}\right) \tag{38}$$

Let $D = \left(-\tilde{\theta}_2 - \tilde{\theta}_1\frac{kRT}{V}\bar{Q}_{Ld} + \tilde{d}_0 - \hat{\zeta}\right)$, the transfer function between e and D can be obtained as follows:

$$\frac{E(s)}{D(s)} = \frac{1}{s + \left(\psi + \frac{h^2(x,t)}{4\delta}\right)} = \frac{\frac{1}{\left(\psi + \frac{h^2(x,t)}{4\delta}\right)}}{\frac{s}{\left(\psi + \frac{h^2(x,t)}{4\delta}\right)} + 1} \tag{39}$$

Obviously, the relationship between e and D can be regarded as the inertia link. The larger the feedback gain Ψ and the smaller the boundary layer thickness δ, the larger the cut-off frequency of the system, the weaker the ability to inhibit the high-frequency dynamics of the system uncertainties. Due to the cut-off frequency of the system is higher, the chattering of the response signal is more serious, which is easy to cause instability of the system. The smaller the feedback gain ψ and the larger the boundary layer thickness δ, the smaller the cut-off frequency, the stronger the attenuation of the high-frequency dynamics, and it can inhibit the chattering of the system, while weaken the responsiveness of the system.

IV. EXPERIMENTS AND ANALYSIS
A. EXPERIMENTAL SETUP
The photograph of the experimental setup is shown in Fig.12. The pneumatic pressure in the chamber (FESTO-80-0.8-SAS0.73 $V = 0.8$L) is used as the controlled
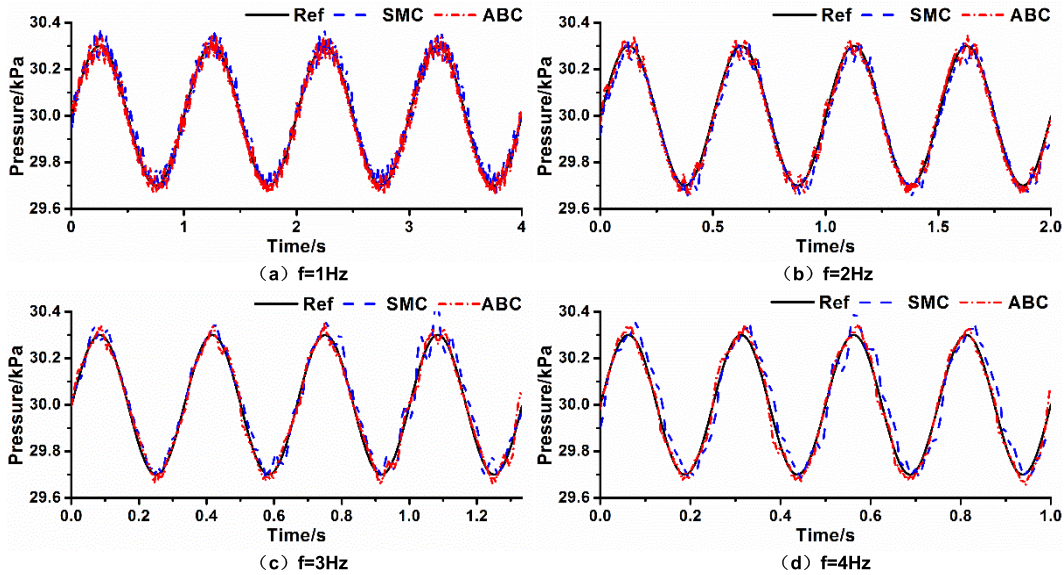
FIGURE 13. Experimental results with SMC and ABC strategy at pressure working point 30kPa.
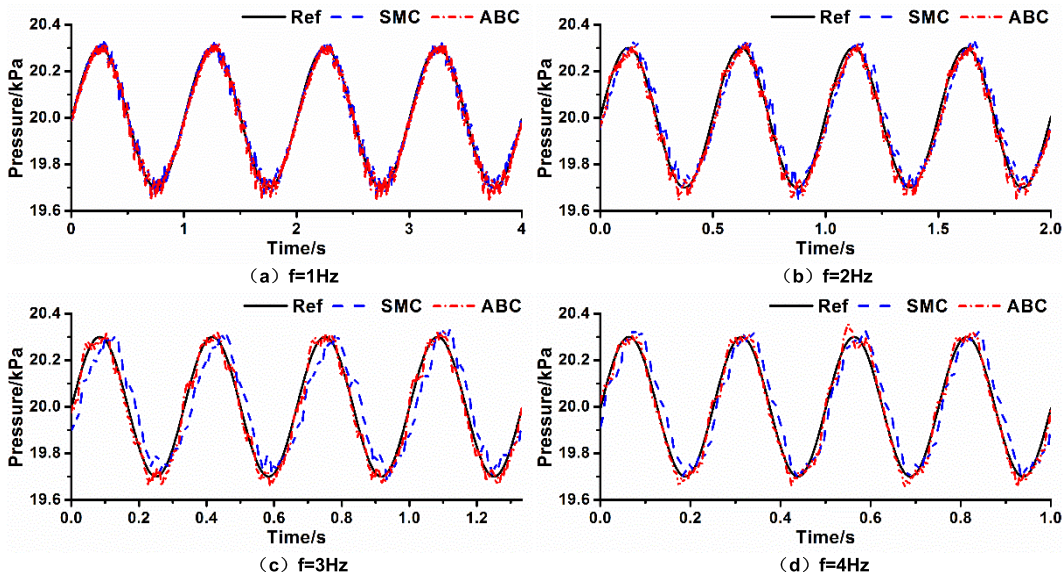

FIGURE 14. Experimental results with SMC and ABC strategy at pressure working point 20kPa.

objective. Two high-precision pressure sensors (Setra 270-RoHS) are used to measure the vacuum pump inlet pressure and the chamber pressure respectively. The charging and discharging units of the system are independent, where in the charging unit uses one V1 HSV (MHE2-MS1H-3/2G-1/8K), and the discharging unit adopts three V2 HSVs (MHE3-MS1H-3/2G-1/8K). The control-data acquisition system including a computer and a high-speed data acquisition card (PCI-1716), which collects the pressure values of the two sensors and generates a PWM signal to drive the solid-state relays (PCLD-786) to control the state of the HSVs.

B. COMPARATIVE EXPERIMENTS

In order to verify whether ABC strategy can guarantee the stability of dynamic vacuum pressure tracking in higher frequency range, the comparision experiments are conducted by using the SMC strategy and ABC strategy in this paper.

1) INTRODUCING THE DESIGN OF SMC

In combination with Eq.(1)-(8) and the duty cycle mapping scheme shown in Fig.11.

$$\frac{dp}{dt} = \frac{kRT}{V} \left(\begin{matrix} 0.0404 \frac{p_{atm}}{\sqrt{T}} S_{cu} f\ (p_{atm}, p)\ (0.5u + 0.5) \\ -0.0404 \frac{p}{\sqrt{T}} S_{du} f\ (p, p_t)\ (-0.5u + 0.5) \end{matrix} \right).$$

(40)

Eq.(40) was transformed into the standard relation of sliding mode variable structure : $\dot{x} = \xi + bu$, in which ξ and b
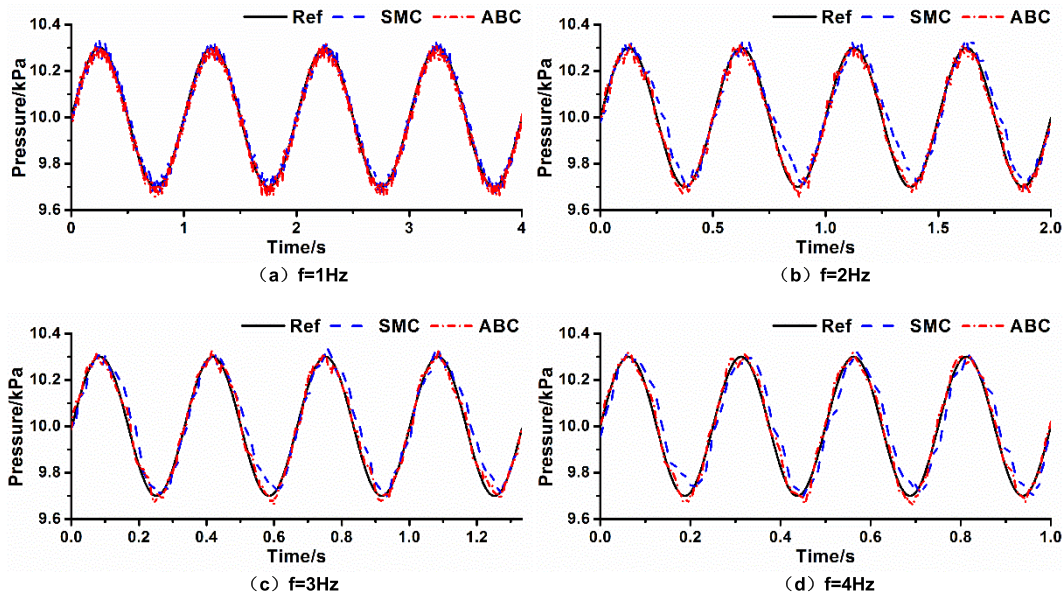
FIGURE 15. Experimental results with SMC and ABC strategy at pressure working point 10kPa.
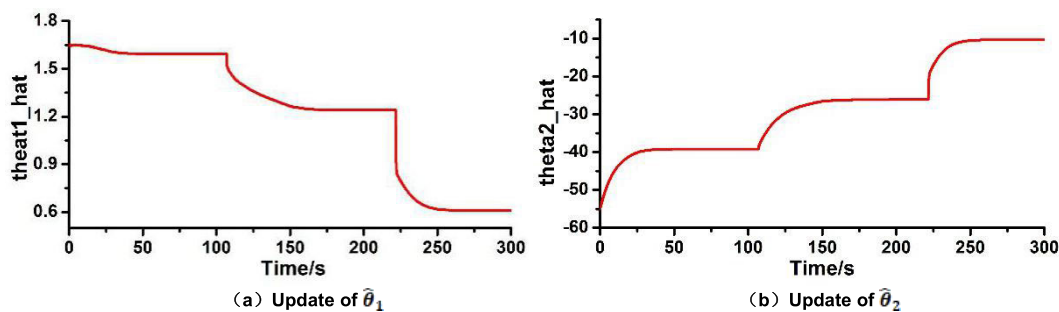

FIGURE 16. Update of parameters $\widehat{\theta}_1$ and $\widehat{\theta}_2$ of ABC strategy.

were expressed as Eq. (41).

$$
\begin{cases}
\xi = \dfrac{kRT}{2V}\left(0.0404\dfrac{p_{atm}}{\sqrt{T}}S_{cu}f\,(p_{atm}, p)\right. \\
\qquad \left. -\,0.0404\dfrac{p}{\sqrt{T}}S_{du}f\,(p, p_t)\right) \\
b = \dfrac{kRT}{2V}\left(0.0404\dfrac{p_{atm}}{\sqrt{T}}S_{cu}f\,(p_{atm}, p)\right. \\
\qquad \left. +\,0.0404\dfrac{p}{\sqrt{T}}S_{du}f\,(p, p_t)\right)
\end{cases}
\tag{41}
$$

The sliding mode switching surface S of the system is designed, as shown in Eq. (42)

$$
S = e + 2\varsigma \int_0^t e\,d\tau + \varsigma^2 \int_0^t \int_0^t e\,d\tau
\tag{42}
$$

In the Eq. (42), e was the tracking error of the system, where $e = p - p_d$, and p_d is the system command signal, ς was the positive definite gain and $\varsigma > 0$.

After deriving Eq.(42), take Eq.(41) into:

$$
\dot{S} = \xi + bu - \dot{p}_d + 2\varsigma e + \varsigma^2 \int_0^t e\,d\tau
\tag{43}
$$

where u was the controller output. Because the system modeling is imprecise, the functions ξ and b in Eq.(41) are not accurate, but the upper and lower bounds of the variation range of the functions ξ and b are a bounded function on p. In practice, the estimated values $\hat{\xi}$ and $\hat{b}$ of ξ and b are used instead, and the requirements are as follows:

$$
\begin{cases}
\left|\xi - \hat{\xi}\right| < F, \ F = F(e, \dot{e}) \\
\hat{b} = \sqrt{(b_{min}b_{max})}
\end{cases}
\tag{44}
$$

In the Eq.(44), the estimation error of F was the error of ξ, which was the function of the error e and its differential. b_{min}, b_{max} are the minimum and maximum values of b, respectively;

In the ideal case, when the system is in sliding mode motion, the system's motion trajectory finally converges to

TABLE 1. Comparison of control effect between SMC and ABC strategy.

SMC/ABC working point frequency	AR (%)	PD (°)	AR (%)	PD (°)	AR (%)	PD (°)
	30kPa		20kPa		10kPa	
1Hz	1.36/0.63	3.64/0.31	2.58/1.13	3.17/0.17	2.62/1.22	3.44/0.20
2Hz	0.5/1.06	5.59/1.26	3.44/2.48	10.02/2.81	7.04/4.31	10.5/3.46
3Hz	0.22/2.55	9.40/0.33	3.78/0.69	14.56/3.57	4.93/2.24	12.77/3.88
4Hz	2.54/6.9	11.43/0.63	4.6/0.54	15.26/4.79	2.95/0.32	16.14/5.35
Note: amplitude ratio and phase difference are abbreviated to AR and PD, respective						

the switching plane $S = 0$ and $\dot{S} = 0$. At this time, the system's equivalent control law of Filippov [27] can be obtained as follows:

$$u_{eq} = -\hat{\xi} + \dot{p}_d - 2\varsigma e - \varsigma^2 \int_0^t e\,d\tau \qquad (45)$$

In order to meet the requirements of variable structure, a discontinuous term needs to be added to Eq.(45), so the system control law u is shown by Eq.(46).

$$u = \hat{b}^{-1}\left(-\hat{\xi} + \dot{p}_d - 2\varsigma e - \varsigma^2 \int_0^t e\,d\tau - K Sign(S)\right) \quad (46)$$

In the formula, K is a time-varying robust gain parameter to ensure that the system quickly converges to the switching plane $S = 0$.

$$K \geq \beta(F + \eta) + |\beta - 1|\,|u_{eq}| \qquad (47)$$

In the formula, the parameter β satisfies $\beta = (b_{\max}/b_{\min})^{1/2}$, and the parameter η is a positive definite parameter, which represents the convergence time, and satisfies:

$$\frac{1}{2}\frac{d}{dt}S^2 \leq -\eta|S| \qquad (48)$$

In order to improve the control accuracy of the system, the chatter phenomenon caused by the *Sign* function in Eq.(46) needs to be suppressed. The saturation function *Sat* is used instead of the *Sign* function to smooth the output of the controller and reduce the chattering phenomenon. After the introduction of the boundary layer ϕ, the boundary layer continually changes the original variable structure, and the discontinuity of the control rate u will be reduced to the neighborhood near the sliding mode switching surface $[-\phi, \phi]$. The relationship between the modified control law and the saturation function is shown in Eq.(49) and (50), respectively:

$$u = \hat{b}^{-1}\left(-\hat{\xi} + \dot{p}_d - 2\varsigma e - \varsigma^2 \int_0^t e\,d\tau - K Sat\left(\frac{S}{\phi}\right)\right) \quad (49)$$

$$Sat\left(\frac{S}{\phi}\right) = \begin{cases} Sign\left(\frac{S}{\phi}\right), & |S| > \phi \\ \frac{S}{\phi}, & |S| \leq \phi \end{cases} \qquad (50)$$

2) ANALYSIS OF EXPERIMENTAL RESULTS

In the experiment, the carrier frequency of the PWM is set to 100Hz, and the sampling frequency is set to 1000Hz. The reference signal for tracking is the sinusoidal curve with a amplitude 300Pa, a frequency of 1Hz, 2 Hz, 3 Hz, 4 Hz, and the pressure working points are 30kPa, 20kPa, and 10kPa, respectively.

The SMC parameters are set as $\varsigma = 0.01$, $\eta = 1$, $\phi = 100$ and the initial values of $b_{\max}$ and $b_{\min}$ are 10 and 0.1, respectively. Those of ABC strategy are set to: $\hat{\theta}_1(0) = 1.65$, $\hat{\theta}_2(0) = -55$, $\hat{\theta}_1 \in [0.1, 1.8]$, $\hat{\theta}_2 \in [-60, -10]$, $\psi = 50$, $\delta = 400$, $\hat{\zeta}(0) = 0$, $\hat{\zeta} \in [-100, 100]$, $v = 10$, $d_{oM} = 10$, $\rho_1 = 0.001$, $\rho_2 = 1$. The air supply pressure is the ambient pressure in the experiments. The experimental results are shown in Fig.13, Fig.14 and Fig.15, amplitude ratio and phase error are shown in Table 1. The reference signal is abbreviated to Ref, amplitude ratio and phase difference are abbreviated to AR and PD, respective. The amplitude ratio(AR) is the ratio of the amplitude of the command signal and the response signal, and the phase difference(PD) is the ratio of the phase difference of the command signal and the response signal. Theoretically, the smaller the amplitude ratio and the phase difference, the better the tracking performance.

It can be seen from Fig.13 that when the tracking frequency is 1-2Hz, the response signals of SMC and ABC both have good tracking performance. However, when the tracking frequency reaches 3-4Hz, the response signal of SMC shows a severe hysteresis when the frequency increases, while the ABC strategy maintains a good tracking performance and achieves much better performance than the SMC. As shown in Fig.14 and 15, the same phenomenon as in Fig.13 becomes increasingly apparent when the pressure working point decreases. Furthermore, when the frequency is 2Hz, SMC also shows severe amplitude error and hysteresis, while the control performance with ABC strategy is basically consistent.

To better illustrate that ABC has better tracking performance than SMC, the amplitude ratio (AR) and phase difference (PD) of SMC and ABC are shown in Table 1. It can

be concluded from Table 1 that when the tracking frequency is 1 Hz, with pressure working points from 30kPa to 10kPa, the increase of AR of SMC strategy is much larger than that of ABC strategy. Furthermore, as the tracking frequency increases, such as the pressure working point at 20 kPa, the tracking frequency is from 1 Hz to 4 Hz, it can be concluded from Table 1 that the PD of the SMC strategy sharply deteriorates.

As shown in Fig.16, it illustrates the update of the parameters $\widehat{\theta}_1$ and $\widehat{\theta}_2$ of the ABC strategy when the pressure working point is 30kpa. The parameters $\widehat{\theta}_1$ and $\widehat{\theta}_2$ are updated online by the adaptive law to inhibit the influence of parametric uncertainties. The parameter $\widehat{\theta}_1$ decreases to a certain position and then converges, while the parameter $\widehat{\theta}_2$ increases to a certain position and then converges. The advantages of on-line update of the uncertain parameters ensure that the ABC strategy can handle the effects of parametric uncertainties in the system under different conditions.

V. CONCLUSION

In this paper, HSVs are used instead of expensive proportional/servo valves as the control components of the vacuum servo system for exploring new control structure. However, due to the delay characteristics of HSVs, the average gas mass flow rate of the HSV has dead zone, saturated zone, and nonlinear zone. Therefore, based on the linear transformation idea, the method of flow linear compensation is designed, so that the average gas mass flow rate of the HSV is approximately positively correlated with the duty cycle of the PWM signal.

In order to balance the charging ability of the charging unit and the discharging ability of the discharging unit, an asymmetric structure is adopted (the discharge unit consists of 3 HSVs and the charging unit has only 1 HSV). The relationship between the duty cycle ddu of discharging unit and the spool duty cycle d_{V2_1}, d_{V2_2} and d_{V2_3} of discharging unit's HSVs is established by the distribution algorithm. The open-loop simulation results show that the average gas mass flow rate $\bar{Q}_{m2}$ of the discharging unit is approximately positively correlated with the duty cycle d_{du} of the discharging unit.

Moreover, the actual vacuum servo system is a nonlinear uncertain system due to the air compression and system leakage. Therefore, an ABC strategy is designed. The robustness of the strategy is used to eliminate the unmodeled dynamics and external disturbances of the system, while the on-line update function of adaptive law is used to inhibit the influence of system's parametric uncertainties. Compared with the experimental results of the SMC strategy, the experimental results show that when the tracking frequency reaches 3-4Hz, the response signal of the ABC strategy will not appear hysteresis. Furthermore, results show that the ABC strategy shows better stable control effect and dynamic tracking performance than SMC strategy. In the tracking process of setting pressure, the ABC strategy can ensure good tracking performance with fast response and high robustness for the vacuum servo system.

REFERENCES

[1] S. Hodgson, M. Quyen Le, M. Tavakoli, and M. Tu Pham, "Sliding-mode control of nonlinear discrete-input pneumatic actuators," in *Proc. IEEE/RSJ Int. Conf. Intell. Robots Syst.*, Sep. 2011, pp. 738–743.

[2] B. K. S. Woods, M. F. Gentry, C. S. Kothera, and N. M. Wereley, "Fatigue life testing of swaged pneumatic artificial muscles as actuators for aerospace applications," *J. Intell. Mater. Syst. Struct.*, vol. 23, no. 3, pp. 327–343, 2010.

[3] B. K. S. Woods, C. S. Kothera, G. Wang, and N. M. Wereley, "Dynamics of a pneumatic artificial muscle actuation system driving a trailing edge flap," *Smart Mater. Struct.*, vol. 23, no. 9, Sep. 2014, Art. no. 095014.

[4] A. Svete, M. Štefe, A. Maček, J. Kutin, and I. Bajsić, "Dynamic pressure generator for dynamic calibrations at different average pressures based on a double-acting pneumatic actuator," *Sens. Actuators A, Phys.*, vol. 247, pp. 136–143, Aug. 2016.

[5] J. Jung, D. Lee, J. S. Kim, and S. I. Han, "Adaptive robust disturbance compensating control for a servo system in the presence of both friction and deadzone," *Proc. Inst. Mech. Eng., C, J. Mech. Eng. Sci.*, vol. 231, no. 3, pp. 432–445, Feb. 2017.

[6] T. Noritsugu and M. Takaiwa, "Robust positioning control of pneumatic servo system with pressure control loop," in *Proc. IEEE Int. Conf. Robot. Autom.*, May 2002, pp. 2613–2618.

[7] N. Igo and K. Hoshino, "Control of offset pressure for pneumatic robots," in *Proc. IEEE/SICE Int. Symp. Syst. Integr. (SII)*, Dec. 2011, pp. 428–433.

[8] J.-C. Renn and C.-M. Liao, "A study on the speed control performance of a servo-pneumatic motor and the application to pneumatic tools," *Int. J. Adv. Manuf. Technol.*, vol. 23, nos. 7–8, pp. 572–576, Apr. 2004.

[9] B. Taheri, D. Case, and E. Richer, "Force and stiffness backstepping-sliding mode controller for pneumatic cylinders," *IEEE/ASME Trans. Mechatronics*, vol. 19, no. 6, pp. 1799–1809, Dec. 2014.

[10] M. Shiee, K. A. Sharifi, M. Fathi, and F. Najafi, "Air pressure control via sliding mode approach using an on/off solenoid valve," in *Proc. 20th Iranian Conf. Elect. Eng.*, May 2012, pp. 857–861.

[11] B. Lu, G. Tao, Z. Xiang, and W. Zhong, "Modeling and control of the pneumatic constant pressure system for zero gravity simulation," in *Proc. IEEE/ASME Int. Conf. Adv. Intell. Mechatronics*, Jul. 2008, pp. 688–693.

[12] X. S. Wang, Y.-H. Cheng, and G.-Z. Peng, "Modeling and self-tuning pressure regulator design for pneumatic-pressure–load systems," *Control Eng. Pract.*, vol. 15, no. 9, pp. 1161–1168, 2007.

[13] X. Li and J. Tang, "Intelligent coordinate control of pneumatic pressure signal generator of airplane engine inlet test system based on fuzzy neural network," in *Proc. Int. Conf. Measuring Technol. Mechatronics Autom.*, Apr. 2009, pp. 503–506.

[14] J. Li, B. Li, and Z. Gao, "Application of PC/104 embedded computer to air pressure control device," in *Proc. IEEE/ASME Int. Conf. Mechtronic Embedded Syst. Appl.*, Oct. 2008, pp. 238–242.

[15] M. Shiee, A. Sharifi K., M. Fathi, and F. Najafi, "An experimental comparison of PWM schemes to improve positioning of servo pneumatic systems," *Int. J. Adv. Manuf. Technol.*, vol. 82, nos. 9–12, pp. 1765–1779, Feb. 2016.

[16] X. Shen, J. Zhang, E. J. Barth, and M. Goldfarb, "Nonlinear averaging applied to the control of pulse width modulated (PWM) pneumatic systems," in *Proc. Amer. Control Conf.*, Jun./Jul. 2004, pp. 4444–4448.

[17] I. Sardellitti, S. Cecchini, S. Silvestri, and D. G. Caldwell, "Proportional mechanical ventilation through PWM driven on/off solenoid valve," in *Proc. Annu. Int. Conf. IEEE Eng. Med. Biol.*, Aug. 2010, pp. 1222–1225.

[18] V. T. Jouppila, S. A. Gadsden, G. M. Bone, A. U. Ellman, and S. R. Habibi, "Sliding mode control of a pneumatic muscle actuator system with a PWM strategy," *Int. J. Fluid Power*, vol. 15, no. 1, pp. 19–31, Jan. 2014.

[19] L. I. Jinyun, "Theoretical and experimental study on the pressure and vacuum continuous control system based on hybrid pump," *Chin. J. Mech. Eng.*, vol. 20, no. 6, pp. 74–78, 2007.

[20] G. Li, B. Li, D. Wu, J. Du, and G. Yang, "Feedback linearization-based self-tuning fuzzy proportional integral derivative control for atmospheric pressure simulator," *Proc. Inst. Mech. Eng., I, J. Syst. Control Eng.*, vol. 228, no. 6, pp. 385–392, Jul. 2014.

[21] X. Cheng, L. Du, G. Yang, and B. Li, "Adaptive robust control of dynamic gas pressure in a vacuum servo system," *Vacuum*, vol. 148, pp. 184–194, Feb. 2018.

[22] G. Yang, K. Chen, L. Du, J. Du, and B. Li, "Dynamic vacuum pressure tracking control with high-speed on-off valves," *Proc. Inst. Mech. Eng., I, J. Syst. Control Eng.*, vol. 232, no. 10, pp. 1325–1336, Nov. 2018.

[23] S. Hodgson, M. Tavakoli, M. T. Pham, and A. Leleve, "Nonlinear discontinuous dynamics averaging and PWM-based sliding control of solenoid-valve pneumatic actuators," *IEEE/ASME Trans. Mechatronics*, vol. 20, no. 2, pp. 876–888, Apr. 2015.

[24] S. Hodgson, M. Q. Le, M. Tavakoli, and M. T. Pham, "Improved tracking and switching performance of an electro-pneumatic positioning system," *Mechatronics*, vol. 22, no. 1, pp. 1–12, Feb. 2012.

[25] M. Chandrapal, X. Chen, W. Wang, and C. Hann, "Nonparametric control algorithms for a pneumatic artificial muscle," *Expert Syst. Appl.*, vol. 39, no. 10, pp. 8636–8644, Aug. 2012.

[26] B. Yao and M. Tomizuka, "Adaptive robust control of MIMO nonlinear systems in semi-strict feedback forms," *Automatica*, vol. 37, no. 9, pp. 1305–1321, Sep. 2001.

[27] B. Yao, "Integrated direct/indirect adaptive robust control of SISO nonlinear systems in semi-strict feedback form," in *Proc. Amer. Control Conf.*, Jun. 2003, pp. 3020–3025.

[28] M. Deyuan, T. Guoliang, L. Aimin, and L. Wei, "Adaptive robust control of high speed switching valve controlled pneumatic position servo system," *J. Mech. Eng.*, vol. 51, no. 10, pp. 180–188, 2015.

[29] G. Yang, L. Du, J. Du, B. Li, and X. Fu, "Convection heat transfer model and verification for the vacuum chamber during charge and discharge processes," *Vacuum*, vol. 139, pp. 67–76, May 2017.

LEI LEI was born in Hunan, China, in 1995. He received the B.S. degree in naval architecture and ocean engineering from Harbin Engineering University (HEU), and the M.S. degree in mechanical engineering from the Huazhong University of Science and Technology (HUST).

From 2016 to 2019, he was a Master with the Institute of Marine Electrical Equipment. His research interests include hydrodynamic optimization and dynamics of robotics and control theory of fluids.

Mr. Lei was awarded Graduate Student with Merit and National Postgraduate Scholarship in HUST.

YONG WU received the master's degree in mechanical engineering from Chongqing University. He was a Famous Expert in the field of machinery and hydraulics, major in mechanical design and theory.

GANG YANG was born in Sichuan, China, in 1973. He received the Ph.D. degree from the School of Mechanical Science and Engineering, Huazhong University of Science and Technology. His main research interests include electro-hydraulic servo/ proportional control technology and electro-pneumatic servo/ proportional control technology.

JINGMIN DU was born in Hubei, China, in 1969. He received the master's degree from the School of Mechanical Science and Engineering, Huazhong University of Science and Technology. His main research interest includes electro-pneumatic servo/ proportional control technology.

PENG JIANG was born in Hunan, China, in 1996. He received the bachelor's degree in mechanical and electronic engineering from the Changsha University of Science and Technology, in 2018. He is currently pursuing the master's degree with the School of Mechanical Science and Engineering, Huazhong University of Science and Technology. His main research interests are pneumatic servo control and electro-hydraulic servo control.

BAOREN LI was born in Liaoning, China, in 1962. He received the Ph.D. degree from the Harbin Institute of Technology. His main research interests include electro-hydraulic servo/ proportional control technology and electro-pneumatic servo/ proportional control technology.

• • •